ac susceptibility study of magnetic relaxation phenomena in the antiskyrmion-hosting tetragonal Mn-Pt(Pd)-Sn system

P. V. Prakash Madduri,[1,*] Subir Sen,[1,*] Bimalesh Giri,[1] Dola Chakrabartty,[1] Subhendu K. Manna,[1] Stuart S. P. Parkin,[2] and Ajaya K. Nayak ⬡[1,†]

[1]*School of Physical Sciences, National Institute of Science Education and Research, HBNI, Jatni 752050, India*
[2]*Max Planck Institute of Microstructure Physics, Weinberg 2, 06120 Halle, Germany*

Here, we report an exhaustive study of the frequency-dependent ac magnetic susceptibility of the D_{2d}-symmetric Heusler system Mn-Pt(Pd)-Sn that hosts antiskyrmions over a wide temperature range. Magnetic relaxation studies using Cole-Cole formalism reveal a Debye-type relaxation with a nearly negligible distribution in relaxation times. In contrast to the archetypical skyrmion hosts, the high Curie temperature T_C of the present system ensures shorter switching times, and correspondingly, higher frequencies are required to probe the relaxation dynamics. We find a nonmonotonic variation in the characteristic relaxation time with distinct maxima at the phase boundaries *via* helical ⟶ antiskyrmion ⟶ field-polarized states, indicating slower magnetization dynamics over the region of phase coexistence. The temperature-dependent relaxation time across different phases is of the order of 10^{-5}–10^{-4} s and follows the well-known Arrhenius law with reasonable values of the energy barriers. The present study concerning the magnetization dynamics in the antiskyrmion host tetragonal Heusler system is an important contribution towards the basic understanding of the dynamical aspects of antiskyrmions for their potential applications.

I. INTRODUCTION

Skyrmions represent a particular class of magnetic *nanodomains* characterized by vortexlike localized spin configurations [1], in contrast to the conventional helical, conical, and spontaneously magnetized spin structures. The twist in the magnetization profile within each domain described by a topological winding number gives robust protection to the spin configurations against continuous deformation [2]. Owing to their solitonic nature, skyrmions can interact efficiently with the electrons and magnons in the host material and result in several exotic electromagnetic phenomena such as topological Hall effect [3], thermally induced ratchet motion [4], and skyrmion magnetic resonance [5]. The competition between the Heisenberg exchange and the Dzyaloshinskii-Moriya (DM) interaction is one of the main reasons behind the observation of skyrmions in bulk and thin-film magnetic systems [3,6–13]. Recently, a new type of topological object named, antiskyrmion, was observed in an acentric tetragonal Heusler Mn-Pt(Pd)-Sn system with D_{2d} crystal symmetry [14]. Note that the high T_C of this material (≈ 400 K) ensures that the antiskyrmions get stabilized over a wide temperature range. In the archetypal skyrmion hosting B20 materials, an externally applied magnetic field favors conical helices propagating along the field direction. In contrast, a particular pattern of DM vectors dictated by the D_{2d} crystallographic symmetry in the Mn-Pt(Pd)-Sn system precludes the emergence of the longitudinal conical structure at finite fields.

In most cases, the presence of the skyrmion phase was identified using small-angle neutron scattering [6], Lorentz transmission electron microscopy (LTEM) [9,14], and, indirectly, by topological Hall transport studies [3,10,15–17]. It is well known that ac susceptibility is a potential technique to identify various magnetic phases and to study their relaxation dynamics [18–20]. Linear and nonlinear susceptibilities with various ac magnetic field amplitudes H_{ac} and frequencies f in the presence and absence of superimposed dc magnetic fields H_{dc} are widely used to unambiguously identify ferro-, ferri-, and antiferromagnetic ordering; the canonical, cluster, and reentrant spin glass nature; spin-reorientation transitions; and superparamagnetism [19,20]. Recently, it was shown that ac susceptibility as a function of dc magnetic field $\chi(H)$ at various fixed frequencies f of the oscillating magnetic field can be used to study the relaxation dynamics of the modulated magnetic phases in different skyrmion host materials that include metallic FeGe [11], MnSi [21], Fe$_{1-x}$Co$_x$Si [22], Mn$_{1-x}$Fe$_x$Si [23]; insulating Cu$_2$OSeO$_3$ [24,25]; and semiconducting GaV$_4$S$_8$ [26]. Peak/hump anomalies in the field evolution of ac susceptibility that characterize the antiskyrmion phase in the tetragonal Heusler Mn-Pt(Pd)-Sn were recently reported [27]. However, detailed studies are required to understand the magnetic relaxation and magnetic phase transitions in such a system. To this end, we have undertaken an in-depth study of high-precision ac susceptibility data on the antiskyrmion hosts Mn$_{1.4}$PtSn and Mn$_{1.4}$Pt$_{0.9}$Pd$_{0.1}$Sn.

II. METHODS

Polycrystalline ingots of Mn$_{1.4}$PtSn and Mn$_{1.4}$Pt$_{0.9}$Pd$_{0.1}$Sn were synthesized using arc-melting technique. Details of the

---

*These authors contributed equally to this work.
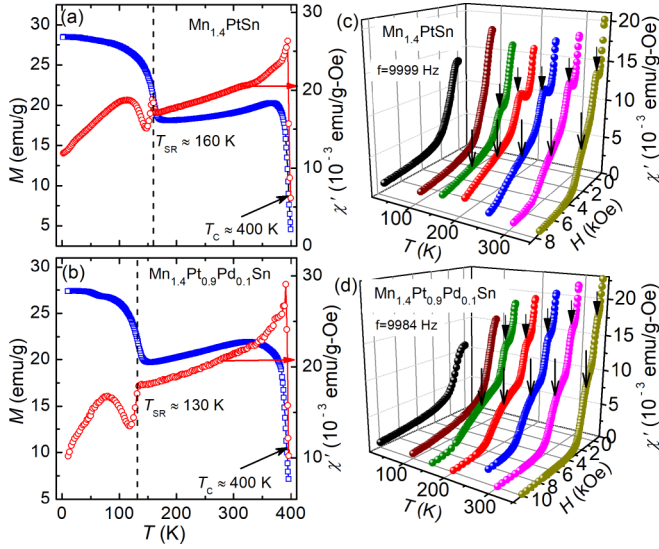†ajaya@niser.ac.in

FIG. 1. Magnetization as a function of temperature $M(T)$ (open squares, left Y axis) measured at $H = 1$ kOe in the field-cooled mode and the temperature-dependent real part of zero-field ac susceptibility curves $\chi'(T)$ shown with open circles (right Y axis) for (a) $Mn_{1.4}PtSn$ and (b) $Mn_{1.4}Pt_{0.9}Pd_{0.1}Sn$. Isothermal field-dependent ac susceptibility curves $\chi(H)$ taken at different temperatures in the range 10 K $\leqslant T \leqslant$ 350 K for (c) $Mn_{1.4}PtSn$ and (d) $Mn_{1.4}Pt_{0.9}Pd_{0.1}Sn$. The evolution of the antiskyrmion phase is inferred from the broad minimum surrounded by maxima in $\chi(H)$ curves. The low-field maximum is well seen by the occurrence of a peak, whereas the high-field maximum is visualized by a spread out hump kind of behavior marked by arrows.
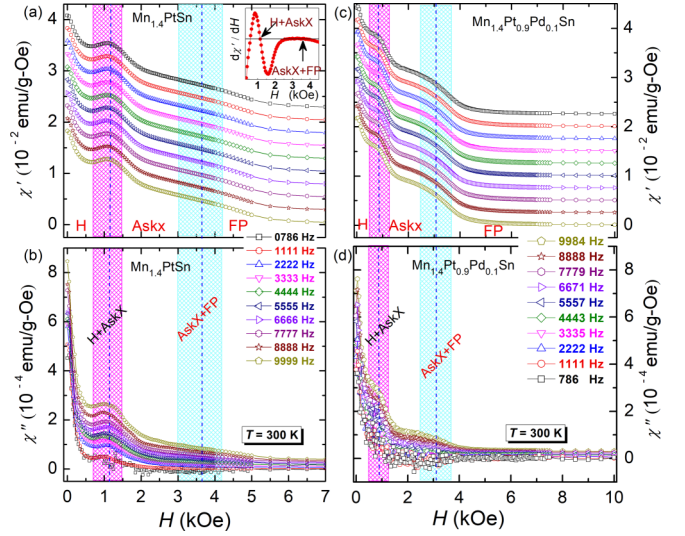

FIG. 2. In-phase [$\chi'(H)$] and out-of-phase [$\chi''(H)$] components of $\chi(H)$ at $T = 300$ K with $H_{ac} = 10$ Oe measured at different frequencies for (a) and (b) $Mn_{1.4}PtSn$ and (c) and (d) $Mn_{1.4}Pt_{0.9}Pd_{0.1}Sn$. Note that for the sake of clarity, the successive $\chi'(H)$ data starting from 8888 Hz have been given a constant upward shift of 2.5 m emu/g Oe. Vertical dashed lines represent the phase crossover from H-AskX and AskX-FP states inferred from $d\chi'/dH$ versus H, as shown in the inset of (a). Shaded regions highlight the coexistence of multiple phases.

sample preparation and structural characterization are provided in the Supplemental Material [28]. Nearly disk-shaped samples of $Mn_{1.4}PtSn$ and $Mn_{1.4}Pt_{0.9}Pd_{0.1}Sn$ with masses of 80.30 and 100.2 mg, respectively, were taken for the ac susceptibility measurements performed on a Quantum Design physical property measurement system. At fixed temperatures T, ac susceptibility χ as a function of the magnetic field H was measured at an rms field H_{ac} of 10 Oe and frequencies f ranging from 11 to 9999 Hz. For each measurement, the sample was "zero-field-cooled" from 400 K ($\approx T_C$) to the desired temperature at a rate of 10 K/min. The in-phase and out-of-phase components of the oscillating magnetization were measured and normalized by the ac drive amplitude H_{ac} to obtain the real (χ') and imaginary (χ'') parts of the ac susceptibility, respectively. Note that during the $\chi(H)$ scan, the magnetic field was stabilized at each step in the *linear approach* mode to achieve high-precision data.

III. RESULTS AND DISCUSSION

$Mn_{1.4}PtSn$ exhibits a T_C of about 400 K and a low-temperature spin-reorientation transition T_{SR} of $\approx$160 K, as depicted in the temperature-dependent magnetization $M(T)$ data plotted in Fig. 1(a). The onset of T_{SR} brings about a sudden change in the magnetization in the $M(T)$ data and a peak/dip kind of behavior in the temperature-dependent real part of the ac susceptibility $\chi'(T)$ curve [Fig. 1(a)]. In the case of $Mn_{1.4}Pt_{0.9}Pd_{0.1}Sn$, T_C is found at a temperature

of about 400 K, and T_{SR} is found at 130 K [Fig. 1(b)]. It has been reported that a change in the magnetic structure below T_{SR} hinders the nucleation process of the antiskyrmion phase [14]. A similar inference has also been made from the field-dependent ac susceptibility and magnetic entropy change measurements in the same materials [27]. Since the antiskyrmion phase in the present system is well established between T_{SR} and T_C, the present work mostly focuses on the ac susceptibility analysis in this particular temperature range. Figures 1(c) and 1(d) show the field-dependent ac susceptibility $\chi(H)$ data measured at different temperatures ranging from 10 to 350 K. The presence of a noticeable peak/dip kind of anomaly in the $\chi(H)$ curves suggests that the applied dc magnetic fields gradually transform the system into different magnetically ordered states. As can be seen, the $\chi(H)$ curve initially starts decreasing with increasing field before exhibiting a maximum in the field range of 1–1.5 kOe for $Mn_{1.4}PtSn$ and 0.6–1.3 kOe for $Mn_{1.4}Pt_{0.9}Pd_{0.1}Sn$ [marked by arrows in the low-field regime of Figs. 1(c) and 1(d)]. Further increasing the field gives rise to a broad humplike behavior in the $\chi(H)$ data [marked by arrows in the intermediate-field regime of Figs. 1(c) and 1(d)], which exhibit a monotonic decreasing trend at higher fields. This broad hump in the $\chi(H)$ data is well pronounced at temperatures close to T_C. The corresponding peak/hump positions signify lower (H_{AskX}^L) and upper (H_{AskX}^H) critical fields that bound the antiskyrmion (AskX) phase. For $H < H_{AskX}^L$, the magnetic state is characterized by a helical spin modulation (H), while for $H > H_{AskX}^H$, it is a collinear/field-polarized (FP) state. It can be noted here that no peak/hump kind of behavior is found for the $\chi(H)$ curves measured at 100 and 2 K, signifying
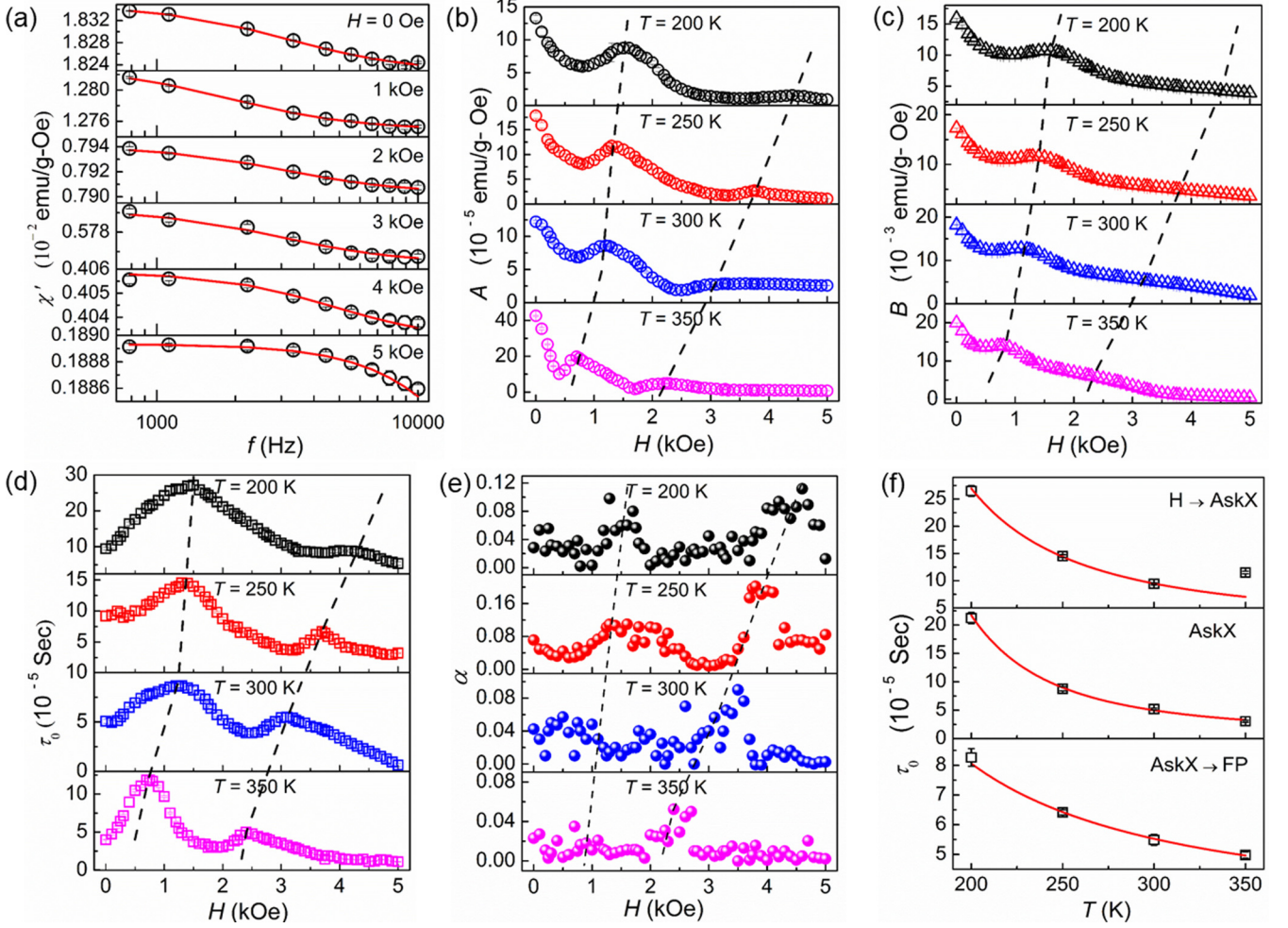
FIG. 3. (a) Frequency dependence of χ' at different representative magnetic fields H measured at $T = 300$ K for Mn$_{1.4}$PtSn. The fits (solid lines) to the data (open symbols) are based on Eq. (1). Magnetic field dependence of the fitting parameters for Mn$_{1.4}$PtSn (b) $A = \chi_T - \chi_S$, (c) $B = \chi_S$, (d) the characteristic relaxation time τ_0, and (e) the relaxation time distribution parameter α. Vertical dashed lines serve as a guide to the eye to indicate the phase boundaries between the H, AskX, and FP phases. (f) Temperature dependence of relaxation time τ_0 derived from (d). τ_0 in the H → AskX and AskX → FP regions are inferred from the lower and upper maxima in the $\tau_0(H)$ plots, whereas $\tau_0(T)$ in the AskX phase is extracted from $\tau_0(H)$ at $H = 2$ kOe. Note that the solid lines represent fits to the observed data (open squares) using Arrhenius's law.

the absence of an antiskyrmion phase in this temperature regime.

The field dependence of $\chi'(H)$ and $\chi''(H)$ data measured at 300 K in the presence of different frequencies is plotted in Fig. 2. As highlighted by the shaded regions, both χ' and χ'' exhibit a hump kind of behavior at the phase transition. Note that the magnitude of $\chi'(H)$ is almost independent of the frequency f of H_{ac}, especially when $f \lesssim 500$ Hz (see Fig. S3) [28]. At low frequencies the $\chi''(H)$ response is so weak that the data are statistically scattered, and no information can be gained. It is also found that the $\chi''(H)$ signal is about two orders of magnitude smaller than that of $\chi'(H)$ and falls close to the instrument resolution limit.

The $\chi'(H)$ data at different frequencies over 786 Hz ⩽ f ⩽ 9999 Hz is replotted as $\chi'(f)$ to systematically investigate the frequency dependency of χ' at various static magnetic fields covering the helical, AskX, and field-polarized magnetic phases. First, we analyze the data for Mn$_{1.4}$PtSn, as shown in Fig. 3(a). The important observations are as follows:

(i) An inflection point in the $\chi'(f)$ data indicates that the relaxation in the antiskyrmion host Mn$_{1.4}$PtSn happens in a frequency window covered in the present experiment.

(ii) In sharp contrast to the skyrmion hosts Fe$_{1-x}$Co$_x$Si [22], Cu$_2$OSeO$_3$ [25], and GaV$_4$S$_8$ [26], where the entire magnetic relaxation is observed in the frequency range over 0.1 Hz to 1 kHz, a frequency window ranging from 0.5 to 10 kHz is needed to study the magnetization dynamics in Mn$_{1.4}$PtSn. A possible reason for the observed behavior could be comparably high T_C (≈ 400 K) that signifies a large exchange energy J in the present system. According to Heisenberg's principle, higher exchange energies lead to shorter switching times as $\tau \propto \hbar/J$. Hence, higher frequencies are needed in order to probe the relaxation dynamics of the present system.

(iii) Noticeable changes are observed in $\chi'(f)$ as one moves gradually from lower to higher magnetic fields. At any given temperature, the inflection point in $\chi'(f)$ shifts to higher frequencies with increasing fields [Fig. 3(a)].

We have attempted to fit the observed variation of $\chi'(f)$ and $\chi''(f)$ data using the well-known Cole-Cole relation [29–31]:

$$\chi'(f) = \chi_S + \frac{A\left[1 + (2\pi f \tau_0)^{1-\alpha} \sin\left(\frac{\pi\alpha}{2}\right)\right]}{1 + 2(2\pi f \tau_0)^{1-\alpha} \sin\left(\frac{\pi\alpha}{2}\right) + (2\pi f \tau_0)^{2(1-\alpha)}},$$
(1)

$$\chi''(f) = \frac{A\left[(2\pi f \tau_0)^{1-\alpha} \cos\left(\frac{\pi\alpha}{2}\right)\right]}{1 + 2(2\pi f \tau_0)^{1-\alpha} \sin\left(\frac{\pi\alpha}{2}\right) + (2\pi f \tau_0)^{2(1-\alpha)}},$$
(2)

where $A = \chi_T - \chi_S$ with $\chi_S \equiv \chi_{f\to\infty}$ and $\chi_T \equiv \chi_{f\to 0}$ representing adiabatic and isothermal susceptibilities, τ_0 is the average relaxation time, and α characterizes the width of the distribution in the relaxation times.

It can be clearly seen from Fig. 3(a) that the fits based on Eq. (1) best represent the observed $\chi'(f)$ data. The fit parameters A, $B \equiv \chi_S$, τ_0, and α are obtained at each field step. The magnetic field variation of the fit parameters at different temperatures is shown in Figs. 3(b)–3(e). The following conclusions can be inferred from the field variation of the fit parameters based on the Cole-Cole formalism.

(i) A nonmonotonic variation is observed in the field dependency of A, $B(\equiv\chi_S)$, τ_0, and α. A broad hump kind of behavior in the field variations of the fit parameters at magnetic field $H = H_1$ [left dashed curves in Figs. 3(b)–3(e)] and H_2 [right dashed curves in Figs. 3(b)–3(e)] is found. These H_1 and H_2 are temperature sensitive and show good agreement with H_{AskX}^L and H_{AskX}^H inferred from $\chi'(H)$, $\chi''(H)$.

(ii) From Fig. 3(b), the parameter $A = \chi_T - \chi_S$ shows broad maxima at $H = H_1$ and H_2. Higher values of A highlight prominent magnetic relaxation in the region of the phase coexistence (helical to AskX and AskX to FP). Butykai *et al.* [26] attributed this kind of behavior to the defects in the magnetization profile arising from the incommensurate spin modulations on the verge of magnetic phase transformation.

(iii) The presence of maxima in $\tau_0(H)$ at $H = H_1$ and H_2 [see Fig. 3(d)] indicates slower magnetization dynamics in the vicinity of the phase transformation that hints at a mixed phase of different magnetic structures. τ_0 at H_1 and H_2 is nearly 1.5 to 3 times higher in comparison to the corresponding values in the pure magnetic phases. In the case of $Fe_{1-x}Co_xSi$ [22], Cu_2OSeO_3 [24,25], and GaV_4S_8 [26], the change in τ_0 is found to be as large as on the order of 10^1 to 10^2. Slower relaxation phenomena characterized by higher relaxation time in the vicinity of phase boundaries signifies a possible origin of irregularities in the spin coordination between different magnetic textures.

(iv) The relaxation time distribution parameter α takes very small values in the range 0.05–0.15. Lower values of α suggest that the relaxation processes of the present magnetic configurations happen nearly in unison. In other words, topologically protected magnetic antiskyrmions, whether in the long-range ordered lattice (AskX phase) phase or in the disordered state (H+Askx phase/FP+Askx phase), undergo almost simultaneous relaxation. Nevertheless, α tends to rise at the phase crossover regions.

(v) Smaller values of $\tau_0 \simeq 10^{-5}$ s, compared to 10^{-3} s reported for the skyrmion host Cu_2OSeO_3, reflect faster relaxation in $Mn_{1.4}PtSn$, presumably due to the large spin-orbit

coupling introduced by the presence of the heavy element Pt in the material. In the absence of quantitative proof, the premise that strong spin-orbit coupling due to Pt is the cause for the faster relaxation times in the present system remains only a conjecture.

(vi) Temperature variation of the characteristic relaxation times corresponding to helical to AskX and AskX to FP phases are plotted in the top and bottom panels of Fig. 3(f). In general, a field of 2 kOe covers the antiskyrmion phase in the whole range of temperatures in the present study. Hence, the temperature dependence of the relaxation time at $H = 2$ kOe is shown in the middle panel of Fig. 3(f). In all cases, the relaxation behavior can be described using the well-known Arrhenius law $\tau_0 \propto \exp(E/k_B T)$, where E characterizes the energy barrier over which the thermal activation takes place. The fits based on the above relation are shown as solid lines to the data presented as symbols. The fitted values yield activation energies (in units of temperature, E/k_B) of 626(30) K, 882(7) K, and 226.5(7.0) K across the H-AskX, AskX, and AskX-FP phases, respectively. A higher value of the energy barrier in the core antiskyrmion lattice region might have resulted from the strong topological protection. Lower values of E at H-AskX, AskX-FP phase boundaries signal metastable antiskyrmions, protected by somewhat lower energy barriers.

While the observation of an antiskyrmion phase in the $Mn_{1.4}PtSn$ system was briefly mentioned earlier, a complete microscopic study was reported in the case of $Mn_{1.4}Pt_{0.9}Pd_{0.1}Sn$ [14]. To further support the present analysis using the Cole-Cole formalism, we have carried out a similar measurement protocol in the case of $Mn_{1.4}Pt_{0.9}Pd_{0.1}Sn$. The frequency dependences of $\chi'(f)$ and $\chi''(f)$ data are fitted using the Cole-Cole relation as discussed earlier [28]. Various fit parameters obtained from the $\chi'(f)$ fitting are plotted in Fig. 4. As can be seen, all the parameters A, B, α, and τ_0 display a well-defined peak in the low-field regime, indicating the nucleation of an antiskyrmion phase with the application of magnetic fields. Similarly, a hump kind of behavior is observed at higher fields for A, B, and τ_0, and a clear peak nature is found in the case of the relaxation time distribution parameter α. In addition, all the fit parameters fall in the same range as that realized in the case of $Mn_{1.4}PtSn$. All these findings further validate the present method of characterizing the antiskyrmion phase in the tetragonal Heusler materials.

It is well known that the out-of-phase component of the ac susceptibility in the Debye-model-like relaxation shows a peak at a characteristic frequency ($f_0 = 1/2\pi\tau_0$). However, in the present case the $\chi''(f)$ data show a shoulder close to f where $\chi'(f)$ goes through an inflection point, as shown in Fig. 5. A complete range of $\chi''(f)$ data at different temperatures and magnetic fields can be found in the Supplemental Material [28]. We have attempted to fit the $\chi''(f)$ data using Eq. (2), as depicted by solid lines in Fig. 5. We use the fit parameters obtained from the $\chi'(f)$ analysis as inputs for the fitting of the $\chi''(f)$ data. Then the parameters were relaxed to obtain the best fitting. However, we could not fit the data in the whole frequency range owing to the lack of a complete peak kind of behavior in the case of both $Mn_{1.4}PtSn$ and $Mn_{1.4}Pt_{0.9}Pd_{0.1}Sn$. A good match between the experimental data and the fitted curve is obtained only up to the frequency where $\chi''(f)$ shows a shoulderlike behavior. This is true for
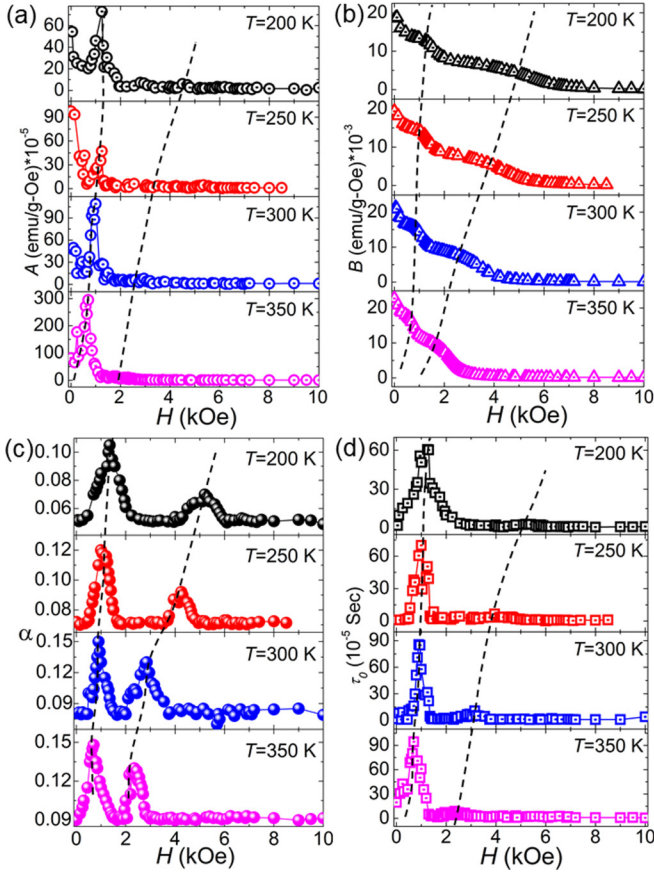
FIG. 4. Field-dependent fitting parameters for $Mn_{1.4}Pt_{0.9}Pd_{0.1}Sn$ (a) $\chi_T - \chi_S$, (b) $B = \chi_S$, (c) α, and (d) τ_0. Dashed lines serve as guide to eye.

FIG. 5. Frequency dependence of χ'' at various representative magnetic fields measured at $T = 300$ K for (a) $Mn_{1.4}PtSn$ and (b) $Mn_{1.4}Pt_{0.9}Pd_{0.1}Sn$. Solid balls represent experimental data points, whereas the lines indicate fits to the data using Eq. (2).

all the temperatures and fields covered in the present study [28]. The fit parameters obtained from the $\chi''(f)$ analysis fall in the same order of magnitude as that found from the $\chi'(f)$ fitting. A comparison of fit parameters acquired from the $\chi'(f)$ and $\chi''(f)$ fittings at 300 K for both $Mn_{1.4}PtSn$ and $Mn_{1.4}Pt_{0.9}Pd_{0.1}Sn$ is presented in Table I. Interestingly, the samples exhibit similar magnitudes of the respective fit parameters, suggesting the presence of similar relaxation dynamics in the present systems. This can be understood from the fact that both the samples display identical magnetic ordering with almost equal T_C.

The deviation of the present $\chi''(f)$ data from the Debye-model-like relaxation could stem from the eddy current losses that adversely affect the susceptibility signals, particularly at higher frequencies and higher dc fields. In general, the voltage induced in the pickup coil by the eddy currents generated in the sample is much smaller when compared to the main voltage induced from the sample in response to the applied ac magnetic field. As a result, the eddy current effect can be clearly seen when the actual signal is very weak [32]. In the present case, the eddy current effect is predominant in the case of $\chi''(f)$ as a signal with a magnitude of $\sim 10^{-5}$–10^{-6} emu/Oe falls in the sensitivity limit of the measuring instrument. A similar magnitude of the eddy current effect of the order of $\sim 10^{-7}$ m^3/mol or $\sim 10^{-5}$ emu/Oe is also found in the $\chi''(f)$ data at 1-kHz frequency in the case of the semiconduct-
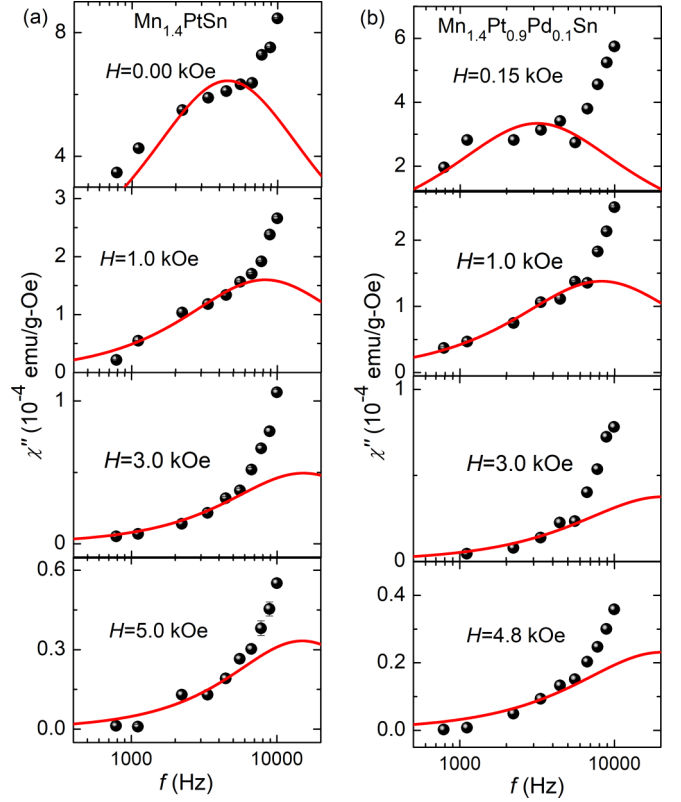
ing skyrmion host $Fe_{1-x}Co_xSi$ [22]. The eddy current effect in the previously studied skyrmion hosting materials could not be seen prominently due to the fact that the magnetic relaxation in these systems happens in the low-frequency regime spanning up to 1 kHz, whereas the present antiskyrmion materials require frequencies up to 10 kHz to study the relaxation process.

It is customary here to compare various magnetic systems that display nontrivial and finite-sized magnetic configurations such as spin glasses, superparamagnetic particles, single-molecule magnets, and skyrmion lattices that exhibit slow magnetic relaxations and are characterized by the Debye relation. Table II compares the typical relaxation times in such systems. In the case of spin glasses, the reorientation of individual magnetic moments or clusters during the relaxation process causes additional frustrations. This results in further rearrangements of the local spins in the system, leading to slower magnetization dynamics. In superparamagnets and single-molecule magnets, slow magnetic relaxation arises from the thermally activated hopping of the spins (macro) over energy barriers dictated by the uniaxial anisotropy which separates parallel and antiparallel configurations. A phase crossover from helical spin modulations to a skyrmion/antiskyrmion lattice is associated with topological point defects [9]. It was reported that the reorientation of large magnetic entities, such as modulations in the long-wavelength spin helices, nucleation of skyrmion cores, and the glassy

TABLE I. Comparison between fitted parameters of χ' and χ'' at 300 K.

H (Oe)	A ($\times 10^{-5}$ emu/g Oe)		τ_0 ($\times 10^{-5}$ s)		α	
	χ'	χ''	χ'	χ''	χ'	χ''
0						
$Mn_{1.4}PtSn$	12.220	149.000	5.070	3.500	0.042	0.092
$Mn_{1.4}Pt_{0.9}Pd_{0.1}Sn$	54.193	122.358	1.536	6.623	0.081	0.080
500						
$Mn_{1.4}PtSn$	7.379	27.071	6.943	3.060	0.057	0.045
$Mn_{1.4}Pt_{0.9}Pd_{0.1}Sn$	15.122	40.136	10.979	3.501	0.103	0.083
1000						
$Mn_{1.4}PtSn$	8.051	36.280	8.287	1.930	0.048	0.080
$Mn_{1.4}Pt_{0.9}Pd_{0.1}Sn$	87.357	26.957	57.727	2.359	0.130	0.082
1500						
$Mn_{1.4}PtSn$	7.340	25.208	8.671	1.682	0.010	0.128
$Mn_{1.4}Pt_{0.9}Pd_{0.1}Sn$	10.476	12.345	1.480	1.214	0.086	0.081
2000						
$Mn_{1.4}PtSn$	3.784	17.365	5.198	1.185	0.036	0.034
$Mn_{1.4}Pt_{0.9}Pd_{0.1}Sn$	5.337	10.251	1.944	0.946	0.107	0.080
2500						
$Mn_{1.4}PtSn$	1.873	13.680	3.880	1.006	0.020	0.051
$Mn_{1.4}Pt_{0.9}Pd_{0.1}Sn$	3.998	8.724	2.516	0.872	0.104	0.083
3000						
$Mn_{1.4}PtSn$	2.761	10.721	5.437	1.048	0.040	0.051
$Mn_{1.4}Pt_{0.9}Pd_{0.1}Sn$	7.762	8.969	6.971	0.989	0.121	0.082
3500						
$Mn_{1.4}PtSn$	2.863	9.767	4.567	1.301	0.090	0.040
$Mn_{1.4}Pt_{0.9}Pd_{0.1}Sn$	3.803	8.113	4.383	0.824	0.092	0.088
4000						
$Mn_{1.4}PtSn$	2.835	7.383	3.389	1.222	0.020	0.070
$Mn_{1.4}Pt_{0.9}Pd_{0.1}Sn$	2.224	6.138	1.314	0.805	0.084	0.085
5000						
$Mn_{1.4}PtSn$	2.584	6.873	0.628	1.067	0.010	0.020
$Mn_{1.4}Pt_{0.9}Pd_{0.1}Sn$	1.253	6.297	1.470	0.854	0.082	0.084

nature of the skyrmion phases [36], leads to slower magnetization dynamics in different skyrmion hosts [21,22,24–26]. Similar phenomena are also expected in the present antiskyrmion host Mn-Pt(Pd)-Sn materials. Higher relaxation time ($\tau_0 \approx 10^{-5}$–10^{-3} s), i.e., a slower relaxation process in the skyrmion/antiskyrmion systems when compared to other systems, signifies a slower magnetic damping process, which suppresses the rate at which an equilibrium configuration can be restored. In this regard, resonance studies of the magnetization dynamics can help us to understand the stability and reliability of future skyrmion/antiskyrmion-based spintronics.

TABLE II. Comparison of relaxation times τ_0 in different magnetic systems.

Magnetic system	τ_0 (s)
Canonical/cluster spin glasses [33]	10^{-12}–10^{-8}
Superparamagnets [34]	10^{-11}–10^{-9}
Single-molecule magnets [35]	10^{-6}
Skyrmion Cu_2OSeO_3 [25] (50 ± 10 nm)	10^{-3}–10^{-2}
Antiskyrmion $Mn_{1.4}Pt(Pd)Sn$ (150 ± 20 nm)	10^{-5}–10^{-4}

H-T phase diagrams are established from the above-discussed features of $\chi'(H)$ and the field-dependent fit parameters of the Cole-Cole relation on the polycrystalline samples $Mn_{1.4}Pt_{0.9}Pd_{0.1}Sn$ and $Mn_{1.4}PtSn$, as shown in Fig. 6. It may be noted here that $H_L^{ACS}(H_L^{Cole-Cole})$ and $H_H^{ACS}(H_H^{Cole-Cole})$ are the lower and upper phase boundaries of the antiskyrmion phase which describe the crossover from the helical state to the antiskyrmion region and the antiskyrmion region to the field-polarized state, respectively. The phase boundaries obtained from the Cole-Cole analysis in the present system broadly match that estimated from the magnetic entropy study [27] and the LTEM technique [14]. The discrepancy seen in the variation of the upper critical fields in the low-temperature regime mostly originates from the nonidentical orientations of the crystallites in the polycrystalline samples used for different measurements. This is due to the fact that the angle between the applied magnetic field and the crystallographic orientation of the crystallites determines the critical field required for the stabilization of antiskyrmions [14]. Hence, depending upon the orientation of the crystallites the critical field for the nucleation of antiskyrmions may vary for different pieces cut from the same sample. The discrepancies in the lower critical fields found between the present study and that of the LTEM investigation [14] can be
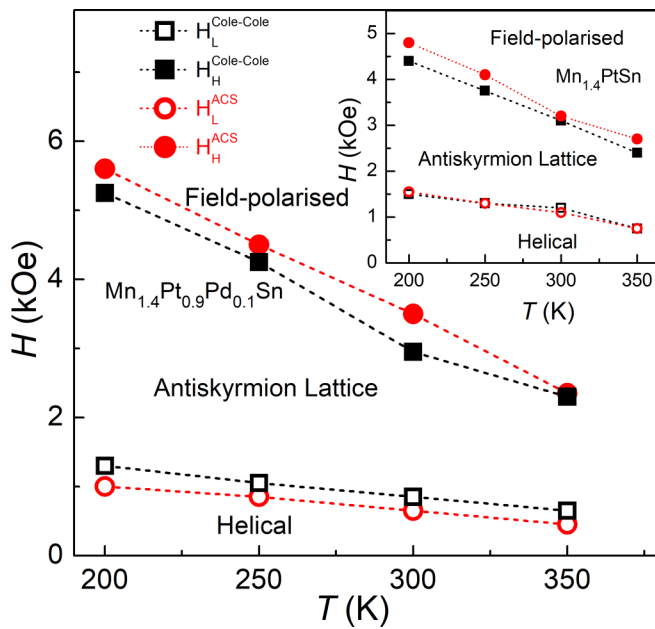
FIG. 6. H-T phase diagram inferred from maxima in the ac susceptibility (circles) and the fit parameters of the Cole-Cole formalism (squares) as described in the text for $Mn_{1.4}Pt_{0.9}Pd_{0.1}Sn$. The inset shows H-T phase diagram for $Mn_{1.4}PtSn$. Open and closed symbols represent the lower and upper boundaries of antiskyrmion phase, respectively. H_L^{ACS} and H_H^{ACS} show the lower and upper phase boundaries of the antiskyrmion phase, respectively, obtained from the peak/hump anomalies in the field evolution of the ac susceptibility measurements. Similarly, $H_L^{Cole-Cole}$ and $H_H^{Cole-Cole}$ are lower and upper phase boundaries of the antiskyrmion phase obtained from the field-dependent fit parameters of the Cole-Cole expression using $\chi'(H)$ data.

understood as follows. In the phase diagram inferred from the LTEM studies, typically, a magnetic field was applied at room temperature to stabilize the antiskyrmion lattice, and then the sample was field-cooled to the required temperature. Subsequently, the magnetic field was slowly varied in different steps, i.e., either reduced to zero or increased to obtain a field-polarized state, and simultaneously monitored the emergence of different magnetic phases. However, in the present case, the sample was *zero-field-cooled* from 400 K to the required

temperature, and the magnetic field strength was continuously raised starting from a zero value to see the field evolution of helical, antiskyrmion, and field-polarized phases. In addition, the Mn-Pt(Pd)-Sn samples used in the LTEM study [14] are [001] oriented 100-nm thin crystalline films prepared with the focused ion beam technique. However, the present ac susceptibility measurements were carried out on the polycrystalline bulk samples. Therefore, it is expected that the phase diagram for the bulk polycrystalline samples may differ slightly in comparison to the single-grain thin-crystalline-film sample.

IV. CONCLUSION

In summary, we have presented a detailed study of the frequency-dependent ac susceptibility measurements on the D_{2d} symmetry based tetragonal Heusler system that hosts an antiskyrmion lattice over a wide temperature range. The magnetic relaxation follows a Debye relation with nearly negligible distribution in the relaxation times. At the boundaries between the different phases via helical to antiskyrmion and antiskyrmion to field-polarized state, the characteristic relaxation time and the isothermal and adiabatic susceptibilities show a nonmonotonic variation. Maxima in the relaxation times that develop in the vicinity of the phase crossover indicate slower magnetization dynamics. Temperature-dependent relaxation times across different magnetic phases follow an Arrhenius kind of slowing down with reasonable values of the energy barriers. The observation of higher relaxation times in comparison to other particulate storage mediums such as superparamagnets and single-molecule magnets signifies a slower damping process in the present antiskyrmion host Mn-Pt(Pd)-Sn system.

[1] U. K. Rößler, A. N. Bogdanov, and C. Pfleiderer, Nature (London) **442**, 797 (2006).

[2] N. Nagaosa and Y. Tokura, Nat. Nanotechnol. **8**, 899 (2013).

[3] A. Neubauer, C. Pfleiderer, B. Binz, A. Rosch, R. Ritz, P. G. Niklowitz, and P. Boni, Phys. Rev. Lett. **102**, 186602 (2009).

[4] M. Mochizuki, X. Z. Yu, S. Seki, N. Kanazawa, W. Koshibae, J. Zang, M. Mostovoy, Y. Tokura, and N. Nagaosa, Nat. Mater. **13**, 241 (2014).

[5] Y. Onose, Y. Okamura, S. Seki, S. Ishiwata, and Y. Tokura, Phys. Rev. Lett. **109**, 037603 (2012).

[6] S. Mühlbauer, B. Binz, F. Jonietz, C. Pfleiderer, A. Rosch, A. Neubauer, R. Georgii, and P. Böni, Science **323**, 915 (2009).

[7] C. Pappas, E. Lelièvre-Berna, P. Falus, P. M. Bentley, E. Moskvin, S. Grigoriev, P. Fouquet, and B. Farago, Phys. Rev. Lett. **102**, 197202 (2009).

[8] W. Münzer, A. Neubauer, T. Adams, S. Mühlbauer, C. Franz, F. Jonietz, R. Georgii, P. Böni, B. Pedersen, M. Schmidt, A. Rosch, and C. Pfleiderer, Phys. Rev. B **81**, 041203(R) (2010).

[9] X. Z. Yu, Y. Onose, N. Kanazawa, J. H. Park, J. H. Han, Y. Matsui1, N. Nagaosa, and Y. Tokura, Nature (London) **465**, 901 (2010).

[10] S. X. Huang and C. L. Chien, Phys. Rev. Lett. **108**, 267201 (2012).

[11] H. Wilhelm, M. Baenitz, M. Schmidt, U. K. Rößler, A. A. Leonov, and A. N. Bogdanov, Phys. Rev. Lett. **107**, 127203 (2011).

[12] S. Seki, X. Z. Yu, S. Ishiwata, and Y. Tokura, Science **336**, 198 (2012).

[13] S. Heinze, K. Bergmann, M. Menzel, J. Brede, A. Kubetzka, R. Wiesendanger, G. Bihlmayer, and S. Blögel, Nat. Phys. **7**, 713 (2011).

[14] A. K. Nayak, V. Kumar, T. Ma, P. Werner, E. Pippel, R. Sahoo, F. Damay, U. K. Rößler, C. Felser, and S. S. P. Parkin, Nature (London) **548**, 561 (2017).

[15] N. Kanazawa, Y. Onose, T. Arima, D. Okuyama, K. Ohoyama, S. Wakimoto, K. Kakurai, S. Ishiwata, and Y. Tokura, Phys. Rev. Lett. **106**, 156603 (2011).

[16] S. X. Huang, F. Chen, J. Kang, J. Zang, G. J. Shu, F. C. Chou, and C. L. Chien, New J. Phys. **18**, 065010 (2016).

[17] S. Sen, C. Singh, P. K. Mukharjee, R. Nath, and A. K. Nayak, Phys. Rev. B **99**, 134404 (2019).

[18] A. H. Morrish, *The Physical Principles of Magnetism* (Wiley, New York, 1965), Chap. 3, pp. 87–101.

[19] M. Balanda, Acta. Phys. Pol. A **124**, 964 (2013), and references therein.

[20] C. V. Topping and S. J. Blundell, J. Phys.: Condens. Matter **31**, 013001 (2019), and references therein.

[21] A. Bauer and C. Pfleiderer, Phys. Rev. B **85**, 214418 (2012).

[22] L. J. Bannenberg, A. J. E. Lefering, K. Kakurai, Y. Onose, Y. Endoh, Y. Tokura, and C. Pappas, Phys. Rev. B **94**, 134433 (2016).

[23] L. J. Bannenberg, F. Weber, A. J. E. Lefering, T. Wolf, and C. Pappas, Phys. Rev. B **98**, 184430 (2018).

[24] I. Levatić, V. Šurija, H. Berger, and I. Živković, Phys. Rev. B **90**, 224412 (2014).

[25] F. Qian, H. Wilhelm, A. Aqeel, T. T. M. Palstra, A. J. E. Lefering, E. H. Brück, and C. Pappas, Phys. Rev. B **94**, 064418 (2016).

[26] Á. Butykai, S. Bordács, L. F. Kiss, B. G. Szigeti, V. Tsurkan, A. Loidl, and I. Kézsmárki, Phys. Rev. B **96**, 104430 (2017).

[27] Sk. Jamaluddin, S. K. Manna, B. Giri, P. V. Prakash Madduri, S. S. P. Parkin, and A. K. Nayak, Adv. Func. Mater. **29**, 1901776 (2019).

[28] See Supplemental Material at http://link.aps.org/supplemental/10.1103/PhysRevB.102.174402 for details of sample preparation, characterization, ac susceptibility analysis, which includes Refs. [18,29–31].

[29] P. Debye, *Polar Moleules* (Chemical Catalog Company, New York, 1929).

[30] H. B. G. Casimir and F. K. Du Pré, Physica **5**, 507 (1938).

[31] K. S. Cole and R. H. Cole, J. Chem. Phys. **9**, 341 (1941).

[32] Y. Kraftmakher, Am. J. Phys. **68**, 375 (2000).

[33] J. A. Mydosh, *Spin Glasses: An Experimental Introduction* (Taylor and Francis, London, 1993).

[34] S. J. Blundell, *Magnetism in Condensed Matter* (Oxford University Press, Oxford, 2001).

[35] L. Thomas, F. Lionti, R. Ballou, D. Gatteschi, R. Sessoli, and B. Barbara, Nature (London) **383**, 145 (1996).

[36] J. Rajeswari, P. Huang, G. F. Mancini, Y. Murooka, T. Latychevskaia, D. McGrouther, M. Cantoni, E. Baldini, J. S. White, A. Magrez *et al.*, Proc. Natl. Acad. Sci. USA **112**, 14212 (2015).